Available online at www.sciencedirect.com
ScienceDirect
Mechanism and Machine Theory 43 (2008) 1317–1331
Mechanism and Machine Theory
www.elsevier.com/locate/mechmt

Contact characteristics of spherical gears

Li-Chi Chao [a], Chung-Biau Tsay [b,*]

[a] Department of Mechanical Engineering, National Chaio Tung University, Hsinchu 30010, Taiwan
[b] Department of Mechanical Engineering, Minghsin University of Science and Technology, Hsinchu 30401, Taiwan

Received 13 October 2006; received in revised form 27 July 2007; accepted 18 October 2007
Available online 11 December 2007

Abstract

In this paper, the theory of gearing and the proposed mechanism of spherical gear cutting are applied to develop the mathematical model of spherical gears. Based on the developed mathematical model of spherical gears, computer graph of the gear set is plotted, and tooth contact analysis (TCA) of spherical gear sets is also performed. The TCA results provide useful information about the kinematic errors (KEs), contact ellipses and contact patterns of spherical gear sets.

Keywords: Spherical gear; Continuous shifting; Tooth contact analysis; Contact ellipse; Kinematic error

1. Introduction

Spherical gear is a new type of gear proposed by Mitome et al. [1]. Geometrically, the spherical gears have two types of gear tooth profiles convex tooth and concave tooth. The convex tooth of spherical gear is similar to a part of ball, and the concave tooth of spherical gear looks like a worm gear. The spherical gear sets have three types of mating assemblies: convex tooth with concave tooth, convex tooth with convex tooth and convex tooth with spur gear. Fig. 1 shows these three types of mating assemblies for the spherical gear set with axial misalignments. Different from the conventional spur or helical gear sets, the spherical gear set allows variable shaft angles and larger axial misalignments without gear interference in meshing. These are two major advantages of spherical gears. Therefore, applying the spherical gear set to replace the gear-type coupling [2] is a good application. Beside, the spherical gear set also can substitute some application occasions of the bevel gear set. The concave tooth of spherical gear can be generated by hobbing with a negative continuous shifting, from both sides of the tooth width to the middle section of gear tooth width, along the rotation axis of the generated gear, whereas the convex tooth of spherical gear can be generated by hobbing with a positive continuous shifting along the gear rotation axis. Moreover, the continuous shifting is in the second order, i.e. an arc. Although the manufacturing method of spherical gears have already been developed, however, only a few of researches on the spherical gears till now. Yang [3] and Yang et al. [4] proposed a ring-involute-teeth

* Corresponding author. Tel.: +886 3 5712121x55128.
E-mail address: cbtsay@mail.nctu.edu.tw (C.-B. Tsay).

0094-114X/$ - see front matter © 2007 Elsevier Ltd. All rights reserved.
doi:10.1016/j.mechmachtheory.2007.10.008

Nomenclature

a, b	tool setting of rack cutter Σ_i
C'	operational center distance
ℓ_i	design parameter on rack cutter ($i = $ F and P)
M_n	normal module
r_j	radius of pitch circle ($j = 1$ and 2)
r	radius of contact ellipse
R_j	spherical radius ($j = 1$ and 2)
S_k (X_k, Y_k, Z_k)	coordinate system k ($k = 1$,2, f, h, m, n, t and v) with three perpendicular axes X_k, Y_k and Z_k
α_n	normal pressure angle
θ_j	spherical angle ($j = 1$ and 2), defined in Fig. 3
θ_t	contact ellipse measurement angle, measured from X_t axis to the radius of searching point of contact ellipse on tangent plane T, defined in Fig. 7
ϕ_j	rotation angle of gear j ($j = 1$ and 2) when gear j is generated by rack cutter
ϕ'_j	rotation angle of gear j ($j = 1$ and 2) when two gears mesh with each other
ΔC	variation of center distance
$\Delta\gamma_h$	horizontal axial misaligned angle
$\Delta\gamma_v$	vertical axial misaligned angle

spherical gear with double degrees of freedom. Tsai and Jehng [5] applied rapid prototyping to form a spherical gear with skew axes. Both spherical gears investigated by Yang and Tsai are different from the spherical gear of this study in generated mechanism, teeth profiles, transmission characteristics and meshing model of gear set.

In the past, many researches have been made for spur gears, helical gears and bevel gears including their respective mathematical models, characteristic analyses, stress analyses and manufactures. Tsay [6] investigated the geometry, computer simulation, tooth contact analysis and stress analysis of the involute helical gear. The spur gear is a special case of helical gears with zero degree of helix angle. Liu and Tsay [7] studied the contact characteristic of bevel gears. Tsai and Chin [8] discussed surface geometry of bevel gears. Litvin et al. [9] probed into low-noise and high-endurance of bevel gears by design, manufacture, stress analysis and experimental tests. The tooth contact analysis (TCA) method was proposed by Litvin [10,11] and Litvin and Fuentes [12], and it had been applied to simulate the meshing of gear drives. The TCA results can provide useful information on contact points, contact ratios and kinematic errors (KEs) of gear sets. The surface separation topology method was proposed by Janninck [13], and it can be applied to determine the contact ellipses on tooth surface of gear sets.

The aim of this paper is to develop the mathematical models of spherical gears with convex teeth and concave teeth. Based on these developed mathematical models, the computer graph of the gear set can be plotted and the TCA is also performed. The instantaneous contact points and kinematic errors of the spherical gear

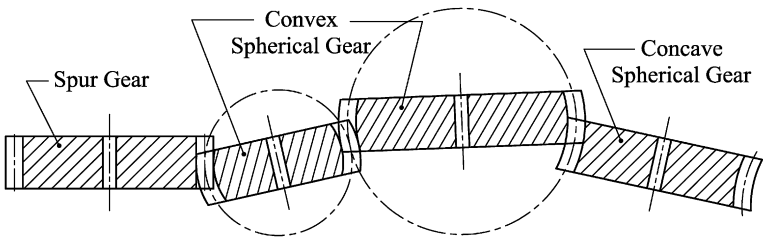

Fig. 1. Mating statuses of spherical gear set with axial misalignments.

can be calculated. In addition, the contact ellipses and contact patterns of spherical sets can also be determined. Some numerical examples are given to illustrate the contact characteristics of the proposed spherical gears.

2. Mathematical model of spherical gears

There are many manufacture methods for gear generation. Hobbing is a popular and efficient method to cut gears. Hobbing method can be applied to cut spur gears, helical gears, bevel gears, etc. It also can be used to cut the spur gear with continuous shifting such as spherical gears. In this study, an imaginary rack cutter is considered to simulate the hobbing process. According to the theory of gearing [10–12] and the gear cutting mechanism, the mathematical model of spherical gears can be developed.

2.1. Mathematical model of rack cutter

The meshing simulation of a spherical gear pair comprises a pinion and a gear. Assume that the rack cutter surfaces Σ_F and Σ_P generate the pinion surface Σ_1 and gear surface Σ_2, respectively. As shown in Fig. 2, the normal section of rack cutter consists mainly of two straight edges, and they can be represented in coordinate system $S_a^{(i)}(X_a^{(i)}, Y_a^{(i)}, Z_a^{(i)})$ by

$$\mathbf{R}_a^{(i)} = \begin{bmatrix} -a + \ell_i \cos \alpha_n \\ \mp(b + a\tan\alpha_n) \pm \ell_i \sin\alpha_n \\ 0 \\ 1 \end{bmatrix} \quad (i = \text{F and P}), \tag{1}$$

where the design parameter $\ell_i = |\overline{M_0M}|(i = \text{F and P})$ represents the distance measured from the initial point M_0 to the moving point M; the symbols M_n and α_n denote the normal module and normal pressure angle of the spherical gear, respectively. The upper and lower signs of Eq. (1) represent the left side and right side surface of rack cutter $\Sigma_i(i = \text{F and P})$, respectively. The symbols a and b are also the design parameters to define the positions of initial point M_0 and moving point M.

Consider that the coordinate system $S_c^{(i)}(X_c^{(i)}, Y_c^{(i)}, Z_c^{(i)})$ is the rack cutter coordinate system, and the profile of rack cutter can be formed by its normal section moving along the hobbing locus of a spherical gear, as shown in Fig. 3. The mathematical model of rack cutter can be determined by using the homogenous coordinate transformation matrix equation transforming from coordinate system $S_a^{(i)}$ to $S_c^{(i)}$. In other words, the rack cutter surface is formed by the hobbing path of the normal section of rack cutter represented in coordinate system $S_c^{(i)}$. Therefore, the rack cutter surface can be represented in coordinate system $S_c^{(i)}$ as follows:

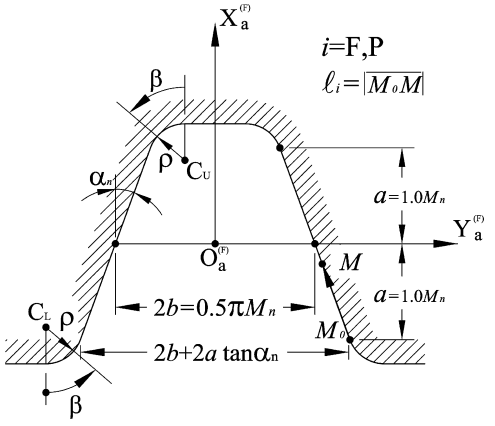

Fig. 2. The normal section of rack cutters Σ_f and Σ_P.

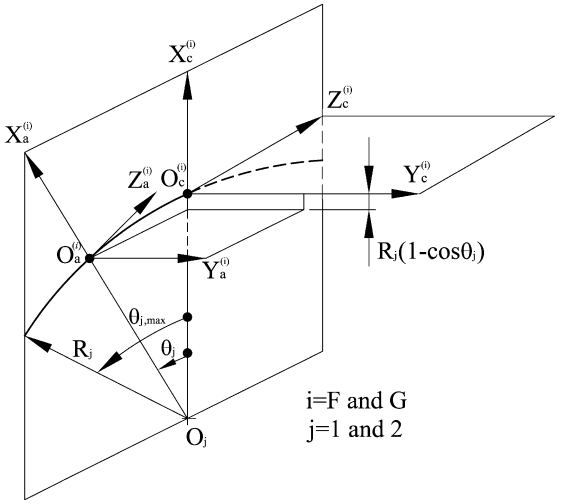

Fig. 3. Relationship between coordinate systems $S_a^{(i)}$ and $S_c^{(i)}$.

$$\mathbf{R}_c^{(i)} = \mathbf{M}_{ca}\mathbf{R}_a^{(i)} = \begin{bmatrix} (-a + \ell_i \cos\alpha_n)\cos\theta_j - R_j(1-\cos\theta_j) \\ \mp(b + a\tan\alpha_n) \pm \ell_i \sin\alpha_n \\ -(-a + \ell_i \cos\alpha_n)\sin\theta_j + R_j \sin\theta_j \\ 1 \end{bmatrix} \quad (i = \mathrm{F}, \mathrm{P} \text{ and } j = 1, 2), \tag{2}$$

where the symbol R_j ($j = 1, 2$) represents the spherical radii and the symbol θ_j ($j = 1, 2$) denotes the spherical angle measured from the central section of spherical gear to the position of normal section of hob cutter at every rotation instant in the gear hobbing process. The upper and lower signs of Eq. (2) represent the left and right sides of the rack cutter surface, respectively.

The normal vector to the rack cutter surface can be attained by

$$\mathbf{N}_c^{(i)} = \frac{\partial \mathbf{R}_c^{(i)}}{\partial \ell_i} \times \frac{\partial \mathbf{R}_c^{(i)}}{\partial \theta_j} \quad (i = \mathrm{F} \text{ and } \mathrm{P} \text{ and } j = 1, 2), \tag{3}$$

where the parameters ℓ_i and θ_j are the surface coordinates of the rack cutter. Eqs. (2) and (3) result in the corresponding normal vector to the rack cutter surface as follows:

$$\mathbf{N}_c^{(i)} = \begin{bmatrix} \pm(a - \ell_i \cos\alpha_n + R_j)\cos\theta_j \sin\alpha_n \\ -(a - \ell_i \cos\alpha_n + R_j \cos 2\theta_j)\cos\alpha_n \\ \mp(a - \ell_i \cos\alpha_n - R_j)\sin\theta_j \sin\alpha_n \end{bmatrix} \quad (i = \mathrm{F}, \mathrm{P} \text{ and } j = 1, 2). \tag{4}$$

Again, the upper and lower signs of Eq. (4) represent the left and right sides of the rack cutter surface, respectively.

2.2. Mathematical model of spherical pinion and gear

According to the theory of gearing [10–12], the mathematical model of the generated tooth surface can be obtained by considering the locus equation of rack cutter surface, expressing in coordinate system of the generated gear, and the equation of meshing. Herein, the locus equation of rack cutter surface can be attained using the homogenous coordinate transformation from the coordinate system of rack cutter to the coordinate system of generated gear. In the gear generation process, gear and cutter surface are never embedded into each other. Thus, the relative velocity of the gear with respect to the cutter, $\mathbf{V}^{(\Sigma g)}$, is perpendicular to their common normal, $\mathbf{N}$. Therefore, the equation of meshing of the gear and rack cutter can be expressed as follows:

$$\mathbf{N} \bullet \mathbf{V}^{(\Sigma g)} = 0, \tag{5}$$

where the superscripts Σ and g denote the rack cutter and generated gear, respectively.

Fig. 4 shows the schematic generation mechanism and the coordinate relationship among the rack cutter and the generated pinion and gear. Herein, the coordinate systems $S_c^{(i)}(X_c^{(i)}, Y_c^{(i)}, Z_c^{(i)}), S_f(X_f, Y_f, Z_f)$, $S_1(X_1, Y_1, Z_1)$ and $S_2(X_2, Y_2, Z_2)$ are attached to the rack cutter, fixed, pinion and gear coordinate systems, respectively. In the generation process, the rack cutter translates to the left with a velocity $\mathbf{V}$ while the pinion rotates with an angular velocity $\boldsymbol{\omega}_1$ and the gear rotates with an angular velocity $\boldsymbol{\omega}_2$, respectively. Thus, both relative velocities of Σ_F with Σ_1 and Σ_P with Σ_2 at the common contact point at every generating instant can be expressed in the fixed coordinate system S_f as follows:

$$\mathbf{V}_f^{(\Sigma_{ij})} = \begin{bmatrix} \pm(r_j\phi_j - Y_c^{(i)})\omega_j \\ \pm X_c^{(i)}\omega_j \\ 0 \end{bmatrix} \quad (i = \mathrm{F}, \mathrm{P} \text{ and } j = 1, 2), \tag{6}$$

where the upper sign of Eq. (6) denotes the relative velocity of Σ_f and Σ_1 while the lower sign denotes the relative velocity of Σ_P and Σ_2. Moreover, the symbols $\Sigma_i (i = \mathrm{F})$ corresponding to $j = 1$ and $\Sigma_i (i = \mathrm{P})$ corresponding to $j = 2$. The symbol ω_j ($j = 1, 2$) denote the angular velocity of the generated pinion ($j = 1$) or gear ($j = 2$). Beside, the terms $X_c^{(i)}$ and $Y_c^{(i)}$ express the X and Y components of position vector $\mathbf{R}_c^{(i)}$, respectively.

According to Eq. (5), the equation of meshing of spherical pinion and gear, expressing in the fixed coordinate system S_f, can be determined and rewritten as follows:

$$\phi_j(\ell_i, \theta_j) = \frac{Y_c^{(i)} N_x^{(i)} - X_c^{(i)} N_y^{(i)}}{r_j N_x^{(i)}}, \tag{7}$$

where symbols $N_x^{(i)}$ and $N_y^{(i)}$ express the X and Y components of normal vector $\mathbf{N}_c^{(i)}$, respectively. Again, the symbol $i = \mathrm{F}$ corresponds to $j = 1$ while $i = \mathrm{P}$ corresponds to $j = 2$.

The locus equation of rack cutter surface, expressing in the coordinate system of generated pinion and gear, can be determined using the homogenous coordinate transformation matrices equation as follows:

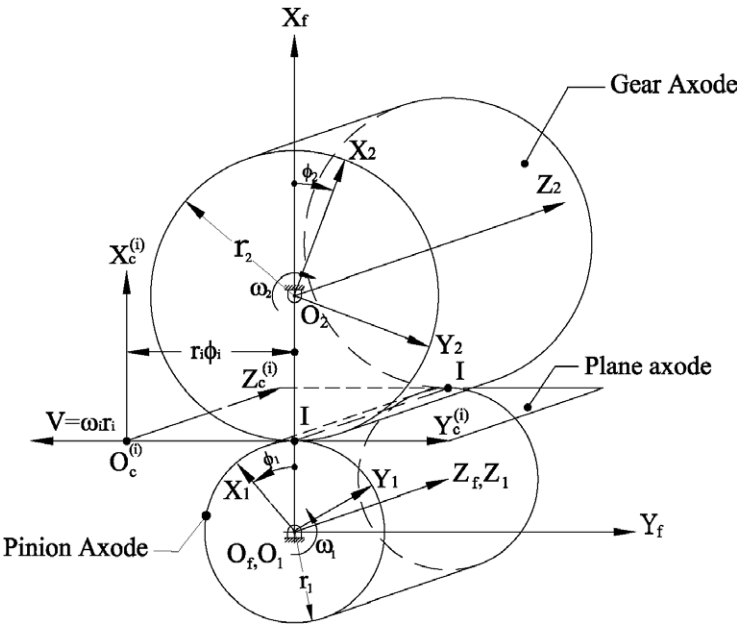

Fig. 4. Coordinate system relationship among rack cutter and generated gears.

$$\mathbf{R}_1 = \mathbf{M}_{1c}\mathbf{R}_c^{(F)} = \begin{bmatrix} \cos\phi_1 & -\sin\phi_1 & 0 & r_1(\cos\phi_1 + \phi_1\sin\phi_1) \\ \sin\phi_1 & \cos\phi_1 & 0 & r_1(\sin\phi_1 - \phi_1\cos\phi_1) \\ 0 & 0 & 1 & 0 \\ 0 & 0 & 0 & 1 \end{bmatrix} \mathbf{R}_c^{(F)}, \tag{8}$$

and

$$\mathbf{R}_2 = \mathbf{M}_{2c}\mathbf{R}_c^{(P)} = \begin{bmatrix} \cos\phi_2 & \sin\phi_2 & 0 & -r_2(\cos\phi_2 + \phi_2\sin\phi_2) \\ -\sin\phi_2 & \cos\phi_2 & 0 & r_2(\sin\phi_2 - \phi_2\cos\phi_2) \\ 0 & 0 & 1 & 0 \\ 0 & 0 & 0 & 1 \end{bmatrix} \mathbf{R}_c^{(P)}. \tag{9}$$

The mathematical models of spherical pinion and gear can be determined by considering Eq. (7) with Eqs. (8) and (7) with (9), respectively. Moreover, the normal vectors of spherical pinion and gear, expressing in their corresponding coordinate systems S_1 and S_2, can be determined as follows:

$$\mathbf{N}_1 = \begin{bmatrix} N_x^{(F)}\cos\phi_1 - N_y^{(F)}\sin\phi_1 \\ N_x^{(F)}\sin\phi_1 + N_y^{(F)}\cos\phi_1 \\ N_z^{(F)} \end{bmatrix}, \tag{10}$$

and

$$\mathbf{N}_2 = \begin{bmatrix} N_x^{(P)}\cos\phi_2 + N_y^{(P)}\sin\phi_2 \\ -N_x^{(P)}\sin\phi_2 + N_y^{(P)}\cos\phi_2 \\ N_z^{(P)} \end{bmatrix}. \tag{11}$$

3. Meshing model and tooth contact analysis

Gear sets are important machine elements for power transmissions. The profile and assembly errors are two main factors that effect the gear transmission performance. The profile errors include the errors of pressure angle, lead angle, tooth profile, etc. These errors relate to the manufacture of gears. Therefore, improving the precision of manufacture is an important issue to increase the gear transmission performance. Another important factor that effects the transmission performance of the gear set is assembly errors. Assembly errors include the errors of center distance, vertical axial misalignment and horizontal axial misalignment. In this paper, the influence of assembly errors on transmission performance is investigated.

3.1. Meshing model of spherical gear set

Fig. 5 shows the schematic diagram that the pinion and gear are meshed with assembly errors. The assembly errors can be simulated by changing the setting of the reference coordinate systems $S_h(X_h, Y_h, Z_h)$ and $S_v(X_v, Y_v, Z_v)$ with respect to the fixed coordinate system. Coordinate systems $S_1(X_1, Y_1, Z_1)$ and $S_2(X_2, Y_2, Z_2)$ are attached to the pinion and gear, respectively. When the gear set is meshed with each other, ϕ_1' and ϕ_2' are the actual rotation angles of the pinion and gear, respectively. To simulate the horizontal axial misalignment of pinion, it can be performed by rotating the coordinate system S_h about axis X_h with a misaligned angle $\Delta\gamma_h$ with respect to coordinate system S_f. Similarly, the simulation of vertical axial misalignment of pinion can be achieved by rotating the coordinate system S_v about axis X_v through a misaligned angle $\Delta\gamma_v$. In addition, the center distance error of spherical set can be performed by moving the coordinate system S_2 along axis X_f through a distance ΔC. Where the symbols $\Delta\gamma_h$, $\Delta\gamma_v$ and ΔC represent the horizontal axial misaligned angle, vertical axial misaligned angle and center distance error of the gear set, respectively.

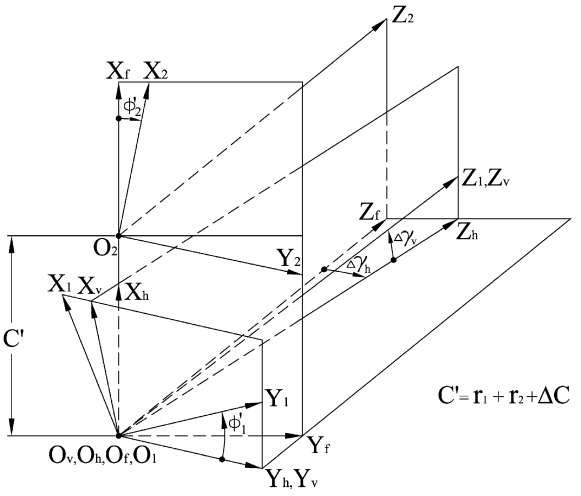

Fig. 5. Spherical gear set of pinion and gear with assembly errors.

3.2. Tooth contact analysis of spherical gear set

According to the tooth contact analysis method [10–12], the position vectors and the unit normal vectors of both pinion and gear should be represented in the same coordinate system, say S_f. The instantaneous common contact point of pinion and gear is the same point in coordinate system S_f. Moreover, the unit normal vectors of the pinion and gear must be collinear to each other. Therefore, the following equations must hold at the point of tangency of the mating gear pair:

$$\mathbf{R}_f^{(1)} - \mathbf{R}_f^{(2)} = 0 \tag{12}$$

and

$$\mathbf{n}_f^{(1)} \times \mathbf{n}_f^{(2)} = 0. \tag{13}$$

In Eq. (12), $\mathbf{R}_f^{(1)}$ and $\mathbf{R}_f^{(2)}$ can be obtained by applying the following equations:

$$\mathbf{R}_f^{(1)} = \mathbf{M}_{fh}\mathbf{M}_{hv}\mathbf{M}_{v1}\mathbf{R}_1, \tag{14}$$

and

$$\mathbf{R}_f^{(2)} = \mathbf{M}_{(f2)}\mathbf{R}_2, \tag{15}$$

where

$$\mathbf{M}_{fh} = \begin{bmatrix} 1 & 0 & 0 & 0 \\ 0 & \cos\Delta\gamma_h & \sin\Delta\gamma_h & 0 \\ 0 & -\sin\Delta\gamma_h & \cos\Delta\gamma_h & 0 \\ 0 & 0 & 0 & 1 \end{bmatrix},$$

$$\mathbf{M}_{hv} = \begin{bmatrix} \cos\Delta\gamma_v & 0 & \sin\Delta\gamma_v & 0 \\ 0 & 1 & 0 & 0 \\ -\sin\Delta\gamma_v & 0 & \cos\Delta\gamma_v & 0 \\ 0 & 0 & 0 & 1 \end{bmatrix},$$

$$\mathbf{M}_{v1} = \begin{bmatrix} \cos\phi_1' & \sin\phi_1' & 0 & 0 \\ -\sin\phi_1' & \cos\phi' & 0 & 0 \\ 0 & 0 & 1 & 0 \\ 0 & 0 & 0 & 1 \end{bmatrix},$$

and

$$\mathbf{M}_{(f2)} = \begin{bmatrix} \cos\phi_2' & -\sin\phi_2' & 0 & C' \\ \sin\phi_2' & \cos\phi_2' & 0 & 0 \\ 0 & 0 & 1 & 0 \\ 0 & 0 & 0 & 1 \end{bmatrix}.$$

$\mathbf{R}_f^{(1)}$ and $\mathbf{R}_f^{(2)}$, respectively represent the position vectors of the pinion and gear, while $\mathbf{n}_f^{(1)}$ and $\mathbf{n}_f^{(2)}$ are the unit normal vectors, represented in coordinate system S_f. Moreover, symbol C' denotes the center distance of spherical gear set with center distance error ΔC, i.e. $C' = r_1 + r_2 + \Delta C$. Since $|\mathbf{n}_f^{(1)}| = |\mathbf{n}_f^{(2)}| = 1$, Eqs. (12) and (13) yield five independent nonlinear equations with six independent parameters $\phi_1', \phi_2', \ell_f, \ell_P, \theta_1$ and θ_2. If the input rotation angle ϕ_1' of the pinion is given, another five parameters can be solved by using a nonlinear solver. By substituting the solved five parameters and ϕ_1' into Eqs. (14) and (15), the contact point of the pinion and gear can be obtained.

The kinematic error (KE) of the spherical gear set can be calculated by applying the following equation:

$$\Delta\phi_2'(\phi_1') = \phi_2'(\phi_1') - \frac{T_1}{T_2}\phi_1', \tag{16}$$

where T_1 and T_2 denote the tooth number of pinion and gear, respectively.

4. Contact patterns

Due to the elasticity of gear tooth surfaces, the tooth surface contact point is spread over an elliptical area. It is known that the instantaneous contact point of the mating gear pair can be determined from the TCA results. When gear drives transmit a power or motion, a set of contact ellipses forms the contact patterns on the tooth surfaces. The simulation methods for contact patterns analysis can be classified into the elastic body method and the rigid body method. The finite element method belongs to the elastic body method for analyzing the contact area with consideration of elastic deformation of tooth surfaces due to the contact stress, thermal stress, and so on. On the other way, the rigid body method for contact patterns analysis includes the curvature analysis method [10–12] and the surface separation topology method [13]. In this study, the contact patterns of spherical gear set are obtained by using the surface separation topology method.

4.1. Contact pattern model

According to the surface separation method, the tooth surfaces of pinion and gear must be transformed from the fixed coordinate system S_f of meshing model to the coordinate system $S_t(X_t, Y_t, Z_t)$. Herein, the coordinate system S_t is attached to the common tangent plane of two contact tooth surfaces at every contact instant. Fig. 6 shows the relationship between the fixed coordinate system S_f and the common tangent plane coordinate system S_t. The coordinate system $S_m(X_m, Y_m, Z_m)$ and $S_n(X_n, Y_n, Z_n)$ are the accessory coordinate systems and they are rotated about the axes X_m and Y_n through the angles δ and ε, respectively. Therefore, the position vectors of pinion and gear tooth surfaces, represented in coordinate system S_t, can be expressed by

$$\mathbf{R}_t^{(j)} = \mathbf{M}_{tn}\mathbf{M}_{nm}\mathbf{M}_{mf}\mathbf{R}_f^{(j)} \quad (j = 1, 2), \tag{17}$$

where

$$\mathbf{M}_{mf} = \begin{bmatrix} 1 & 0 & 0 & -p_x \\ 0 & 1 & 0 & -p_y \\ 0 & 0 & 1 & -p_z \\ 0 & 0 & 0 & 1 \end{bmatrix},$$

$$\mathbf{M}_{nm} = \begin{bmatrix} 1 & 0 & 0 & 0 \\ 0 & \cos\delta & -\sin\delta & 0 \\ 0 & \sin\delta & \cos\delta & 0 \\ 0 & 0 & 0 & 1 \end{bmatrix},$$

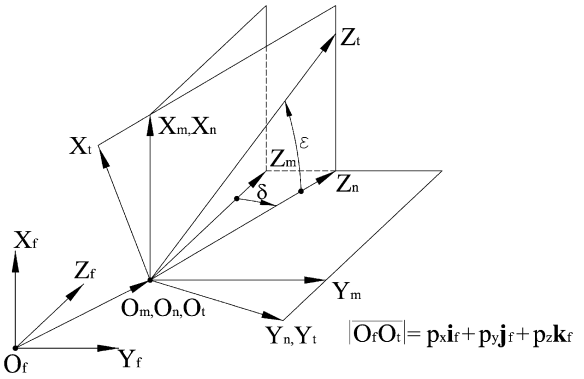

Fig. 6. Coordinate system relationship of contact point and tangent plane.

$$\mathbf{M}_{tn} = \begin{bmatrix} \cos\varepsilon & 0 & -\sin\varepsilon & 0 \\ 0 & 1 & 0 & 0 \\ \sin\varepsilon & 0 & \cos\varepsilon & 0 \\ 0 & 0 & 0 & 1 \end{bmatrix},$$

and the angle formed by axes Z_m and Z_n is $\delta = \tan^{-1}\left(\frac{n_{fy}^{(j)}}{n_{fz}^{(j)}}\right)$, and angle formed by axes Z_n and Z_t is $\varepsilon = \tan^{-1}\left(\frac{n_{fx}^{(j)}}{\sqrt{n_{fy}^{(j)2}+n_{fz}^{(j)2}}}\right)$. The symbols $n_{fx}^{(j)}, n_{fy}^{(j)}$ and $n_{fz}^{(j)}$ are three components of unit normal vectors of spherical pinion and gear surfaces expressed in the fixed coordinate system S_f, where the superscript "j" denotes the spherical pinion ($j = 1$) and spherical gear ($j = 2$). Moreover, symbols p_x, p_y and p_z are the three components of the position vector of common contact point O_t represented in fixed coordinate system S_f.

4.2. Simulation of contact ellipses

Fig. 7a shows the contact tooth surfaces of pinion Σ_1 and gear Σ_2 which tangent to each other at their instantaneous contact point O_t. It is noted that the instantaneous contact point O_t can be determined by the TCA computation. In Fig. 7, the symbol **n** represents the unit normal vector of pinion Σ_1 represented in coordinate system S_t and coincides with the Z_t axis. The calculation of contact ellipse is based on the TCA results and polar coordinates concept. The geometric center of a contact ellipse is the instantaneous contact point of two mating tooth surfaces, determined by the TCA results. The geometric center is considered as the origin of the polar coordinate system. To determine a contour point on the contact ellipse, one should search a pair of polar coordinates (r, θ_t), as shown in Fig. 7a, beginning from axis X_t with an increment angle for θ_t, say 10°. The symbol r represents the position (polar coordinate) of the contact ellipse at the corresponding polar coordinate θ_t, expressed in the coordinate system S_t, and is located on the common tangent plane. The value of every position point r of contact ellipse must satisfy the separation distance $(d_1 + d_2) = 0.00632$ mm. Since the coating paint on the pinion tooth surfaces for bearing contact test will be scraped away and printed on the gear surfaces when the distance, measured along Z_t axis, of two mating tooth surfaces (Σ_1 and Σ_2) is less than the paint's diameter, as shown in Fig. 7b. Since the diameter of coating paint for bearing contact test is 0.00632 mm, therefore, the separation distance is set to equal the diameter of the coating paint for simplicity. Herein, the symbol d_1 is the distance, measured along Z_t direction, of Σ_1 and common tangent plane T, whereas the symbol d_2 is the distance between Σ_2 and common tangent plane T. Therefore, the contact ellipse can be determined by applying the following equations:

$$X_t^{(1)} = r\cos\theta_t = X_t^{(2)} \quad (-\pi \leqslant \theta_t \leqslant \pi), \tag{18}$$

$$Y_t^{(1)} = r\sin\theta_t = Y_t^{(2)} \quad (-\pi \leqslant \theta_t \leqslant \pi), \tag{19}$$

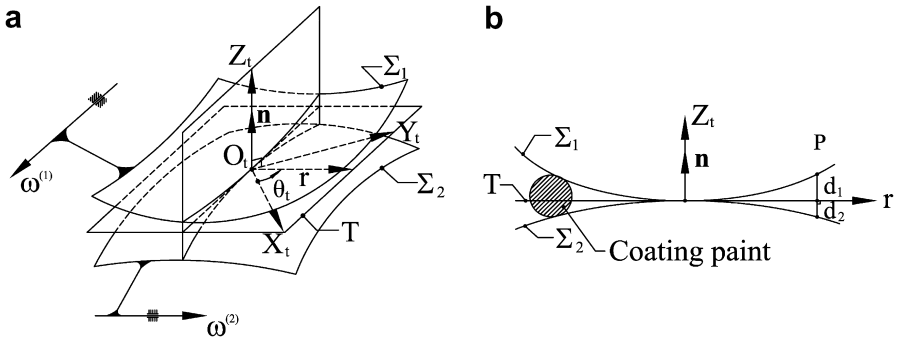

Fig. 7. (a) Common tangent plane and polar coordinates. (b) Separation distances between pinion and gear surfaces.

and

$$|Z_t^{(1)} - Z_t^{(2)}| = 0.00632 \text{ mm}. \tag{20}$$

Thus, the position and size of contact ellipses of the spherical gear set can be determined by using Eqs. (18)–(20).

5. Numerical examples

Based on the mathematical model and meshing model of the spherical gears, the gear tooth profiles can be plotted and computer simulations of spherical gear sets can be performed.

Example 1. Computer graphs of the convex spherical pinion and concave spherical gear

The major spherical gear parameters are given in Table 1. Based on the developed mathematical model of spherical gears, the three-dimensional mating model of spherical pinion and gear can be plotted. Fig. 8 illustrates the mating model of the convex spherical pinion and the concave spherical gear.

Example 2. Convex spherical pinion vs. concave spherical gear

The major spherical gear parameters are the same as given in Table 1. The gear pair is composed of convex spherical pinion and concave spherical gear, and assembled with three conditions as follows:

Case 1. $\Delta\gamma_h = \Delta\gamma_v = 0^\circ$ and $\Delta C = 0$ mm (ideal assembly condition).

Case 2. $\Delta\gamma_h = \Delta\gamma_v = 0^\circ$ and $\Delta C = 0.2$ mm (0.25% center distance variation).

Case 3. $\Delta\gamma_h = -0.05^\circ$, $\Delta\gamma_v = 2.0^\circ$ and $\Delta C = 0.2$ mm (0.25% center distance variation).

Case 1 is the ideal assembly condition. Case 2 indicates that the gear set has the error of center distance. Case 3 indicates that the gear set has both the axial misalignments and error of center distance. The simulated kinematic errors (KEs) and bearing contacts of these cases are shown in Table 2 and Fig. 9, respectively. By

Table 1
Major design parameters of spherical pinion and gear

	Pinion	Gear		
Type of gears	Spherical convex	Spherical concave	Spherical convex	Spur
Normal module (mm/teeth)	2	2	2	2
Normal pressure angle (deg.)	20	20	20	20
Number of teeth	33	47	47	47
Spherical angle θ_j (deg.)	±13.137	±9.182	±9.182	–
Face width (mm)	15	15	15	15

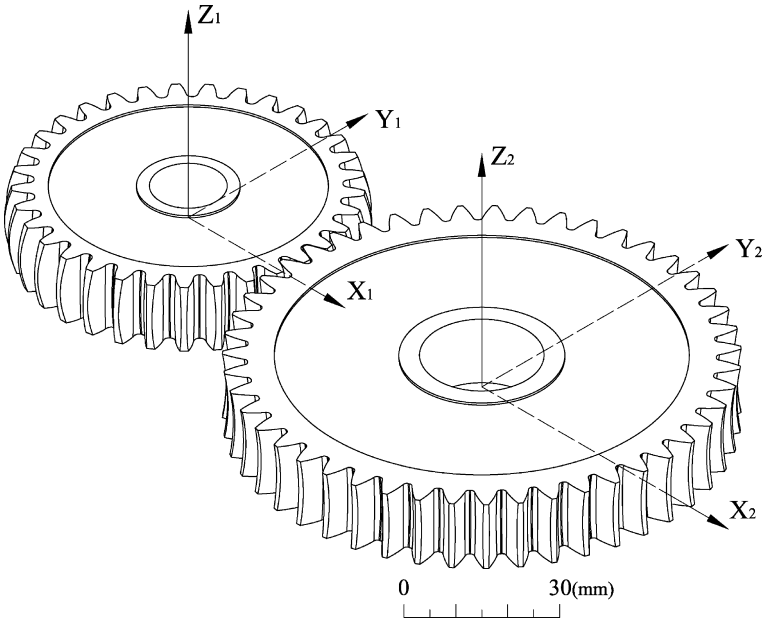

Fig. 8. Computer graph of the convex spherical pinion and the concave spherical gear.

Table 2
Kinematic errors and bearing contacts for spherical gear set with convex pinion and concave gear

Case	ϕ_1' (deg.)	ϕ_2' (deg.)	ℓ_f (mm)	ℓ_P (mm)	θ_1 (deg.)	θ_2 (deg.)	K.E. (arc-sec)
1	−6.0000	−4.2128	1.4837	1.4837	0.0000	0.0000	0.0000
	−3.0000	−2.1064	2.0746	2.0746	0.0000	0.0000	0.0000
	0.0000	0.0000	2.6656	2.6656	0.0000	0.0000	0.0000
	3.0000	2.1064	3.2566	3.2566	0.0000	0.0000	0.0000
	6.0000	4.2128	3.8475	3.8475	0.0000	0.0000	0.0000
2	−6.0000	−4.2128	1.5603	1.3494	0.0000	0.0000	0.0000
	−3.0000	−2.1064	2.1513	1.9404	0.0000	0.0000	0.0000
	0.0000	0.0000	2.7422	2.5314	0.0000	0.0000	0.0000
	3.0000	2.1064	3.3332	3.1223	0.0000	0.0000	0.0000
	6.0000	4.2128	3.9242	3.7133	0.0000	0.0000	0.0000
3	−6.0000	−4.2109	1.5724	1.3647	2.9219	0.6934	6.7400
	−3.0000	−2.1056	2.1615	1.9498	2.5096	0.3537	2.9448
	0.0000	0.0000	2.7509	2.5367	2.1275	0.0367	0.0000
	3.0000	2.1058	3.3408	3.1253	1.7727	−0.2600	−2.1607
	6.0000	4.2118	3.9312	3.7157	1.4426	−0.5384	−3.5930

substituting the solved parameters ϕ_1', ℓ_f and θ_1 into Eq. (14), the contact point on the pinion tooth surface is obtained. Similarly, substituting the solved parameters ϕ_2', ℓ_P and θ_2 into Eq. (15), the contact point on the gear tooth surface is obtained.

In the ideal assembly condition (Case 1), the gear set has no KE and tooth surfaces contact to each other at the middle section of the face width, i.e. $\theta_1 = \theta_2 = 0°$. In Case 2, the gear pair also has no KE and they contact to each other at the middle section of the face width. Case 3 has a little higher level of KEs than other two cases under the condition with axial misalignments and center distance error. Due to the profiles at the middle section of spherical pinion and gear are the same as that of the spur gear with no shifting, therefore, the contact characteristic at the middle section of spherical gear set is similar to that of the spur gear. The only different between spherical gear and spur gear is that the spherical gear set is in point contact and the spur gear is in line contact. Fig. 9 illustrates the loci of contact points and their corresponding contact ellipses on the

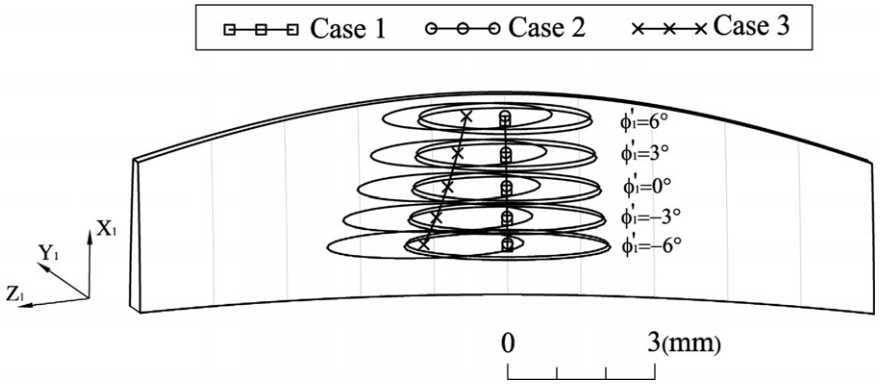

Fig. 9. Contact patterns of spherical gear set with convex pinion and concave gear.

pinion tooth surface for the above-mentioned three cases. The positions of contact points and contact ellipses of spherical gear set for Cases 1 and 2 are almost the same and are located at the middle section of the face width. However, the contact points and contact ellipses are slightly departed from the middle section of the face width for Case 3.

Example 3. Convex spherical pinion vs. convex spherical gear

The major spherical gear parameters are also shown in Table 1. This example investigates the meshing simulations of the spherical gear set with convex pinion and convex gear under the following assembly conditions:

Case 4. $\Delta\gamma_h = \Delta\gamma_v = 0°$ and $\Delta C = 0$ mm (ideal assembly condition).

Case 5. $\Delta\gamma_h = \Delta\gamma_v = 0°$ and $\Delta C = 0.2$ mm (0.25% center distance variation).

Case 6. $\Delta\gamma_h = -0.05°$, $\Delta\gamma_v = 2.0°$ and $\Delta C = 0.2$ mm (0.25% center distance variation).

Table 3 summarizes the simulated results of the bearing contacts and KEs of Cases 4–6, and Fig. 10 illustrates the loci of contact points and their corresponding contact ellipses on the pinion tooth surface. In Cases 4 and 5, the KEs remain zero and the loci of contact points are also located at the middle section of the face width which are the same as those of Cases 1 and 2. As to Case 6, there is a lower level of KEs induced,

Table 3
Kinematic errors and bearing contacts for spherical gear set with convex pinion and gear

Case	ϕ_1' (deg.)	ϕ_2' (deg.)	ℓ_f (mm)	ℓ_P (mm)	θ_1 (deg.)	θ_2 (deg.)	K.E. (arc-sec)
4	−6.0000	−4.2128	1.4837	1.4837	0.0000	0.0000	0.0000
	−3.0000	−2.1064	2.0746	2.0746	0.0000	0.0000	0.0000
	0.0000	0.0000	2.6656	2.6656	0.0000	0.0000	0.0000
	3.0000	2.1064	3.2566	3.2566	0.0000	0.0000	0.0000
	6.0000	4.2128	3.8475	3.8475	0.0000	0.0000	0.0000
5	−6.0000	−4.2128	1.5603	1.3494	0.0000	0.0000	0.0000
	−3.0000	−2.1064	2.1513	1.9404	0.0000	0.0000	0.0000
	0.0000	0.0000	2.7422	2.5314	0.0000	0.0000	0.0000
	3.0000	2.1064	3.3332	3.1223	0.0000	0.0000	0.0000
	6.0000	4.2128	3.9242	3.7133	0.0000	0.0000	0.0000
6	−6.0000	−4.2114	1.5653	1.3568	2.1054	0.1243	4.7680
	−3.0000	−2.1057	2.1579	1.9467	2.0970	0.0661	2.4149
	0.0000	0.0000	2.7506	2.5365	2.0851	0.0071	0.0000
	3.0000	2.1057	3.3432	3.1262	2.0697	−0.0525	−2.4673
	6.0000	4.2114	3.9359	3.7158	2.0510	−0.1127	−4.9774

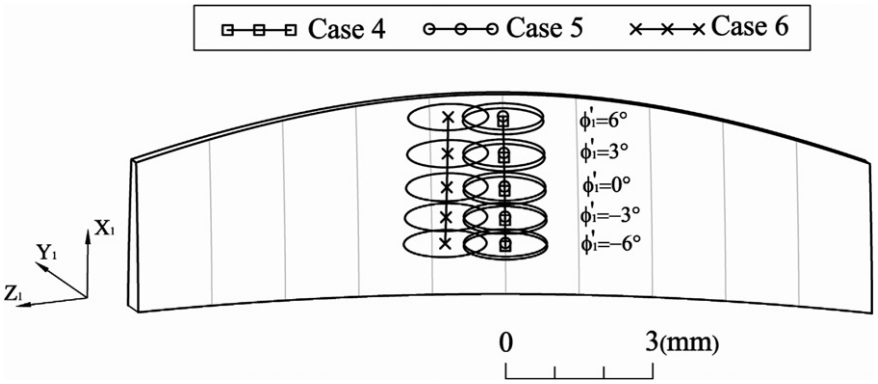

Fig. 10. Contact patterns of spherical gear set with convex pinion and convex gear.

and the contact points and contact ellipses are also slightly departed from the middle section of the face width. It is noted that the meshing models of spherical gear sets in Cases 4–6 are convex spherical pinion mating with convex spherical gear, therefore, the sizes of contact ellipses are smaller than those of Cases 1–3.

Example 4. A gear set with convex spherical pinion and spur gear

The major gear parameters are given in Table 1. This example investigates the meshing simulations of the gear set with convex spherical pinion and spur gear under the following assembly conditions:

Case 7. $\Delta\gamma_h = \Delta\gamma_v = 0°$ and $\Delta C = 0$ mm (ideal assembly condition).

Case 8. $\Delta\gamma_h = \Delta\gamma_v = 0°$ and $\Delta C = 0.2$ mm (0.25% center distance variation).

Case 9. $\Delta\gamma_h = -0.05°$, $\Delta\gamma_v = 2.0°$ and $\Delta C = 0.2$ mm (0.25% center distance variation).

Table 4 summarizes the simulated results of the bearing contacts and KEs of Cases 7–9, while Fig. 11 illustrates the loci of contact points and their corresponding contact ellipses on the pinion surface. For the cases of ideal assembly condition (Case 7) and center distance error condition (Case 8), the contact positions are the same as those of Cases 1 and 2 of Example 2 and Cases 4 and 5 of Example 3, since the tooth profiles at the

Table 4
Kinematic errors and bearing contacts for spherical gear set with convex pinion and spur gear

Case	ϕ_1'(deg.)	ϕ_2'(deg.)	ℓ_f (mm)	ℓ_P (mm)	θ_1 (deg.)	θ_2 (deg.)	K.E. (arc-sec)
7	−6.0000	−4.2128	1.4837	1.4837	0.0000	0.0000	0.0000
	−3.0000	−2.1064	2.0746	2.0746	0.0000	0.0000	0.0000
	0.0000	0.0000	2.6656	2.6656	0.0000	0.0000	0.0000
	3.0000	2.1064	3.2566	3.2566	0.0000	0.0000	0.0000
	6.0000	4.2128	3.8475	3.8475	0.0000	0.0000	0.0000
8	−6.0000	−4.2128	1.5603	1.3494	0.0000	0.0000	0.0000
	−3.0000	−2.1064	2.1513	1.9404	0.0000	0.0000	0.0000
	0.0000	0.0000	2.7422	2.5314	0.0000	0.0000	0.0000
	3.0000	2.1064	3.3332	3.1223	0.0000	0.0000	0.0000
	6.0000	4.2128	3.9242	3.7133	0.0000	0.0000	0.0000
9	−6.0000	−4.2114	1.5661	1.3577	2.2364	0.1769	5.0831
	−3.0000	−2.1057	2.1584	1.9471	2.1629	0.0919	2.4994
	0.0000	0.0000	2.7506	2.5365	2.0918	0.0097	0.0000
	3.0000	2.1057	3.3428	3.1260	2.0230	−0.0699	−2.4191
	6.0000	4.2114	3.9349	3.7155	1.9564	−0.1470	−4.7617

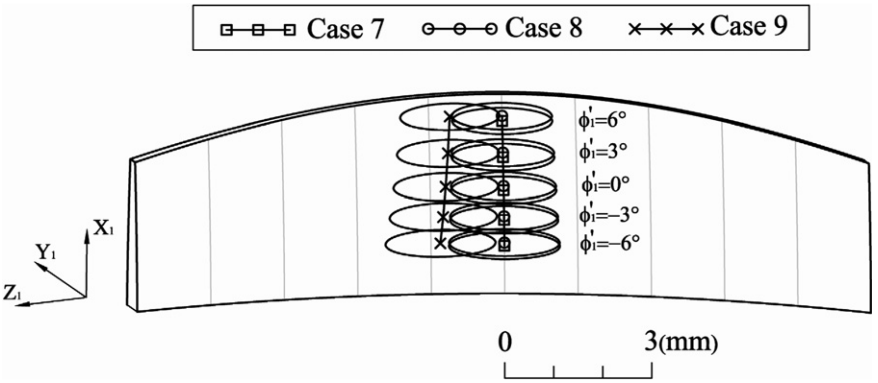

Fig. 11. Contact patterns of a gear set with spherical convex pinion and spur gear.

Table 5
Average ratio a/b of major and minor axes of the contact ellipses of spherical sets with different tooth pressure angles

Pressure angle (deg.)	14.5	20.0	25.0
Convex pinion vs. concave gear			
Case 10	9.339	6.705	5.377
Case 11	9.048	6.586	5.315
Convex pinion vs. convex gear			
Case 10	4.029	2.901	2.334
Case 11	4.011	2.893	2.330
Convex pinion vs. spur gear			
Case 10	5.194	3.731	2.994
Case 11	5.151	3.711	2.985

middle section of the face width of convex tooth and concave tooth are the same as that of the spur gear. However, the size of contact ellipses of this example is smaller than those of Cases 1 and 2 of Example 2, but larger than those of Cases 4 and 5 of Example 3.

Example 5. Average ratio a/b of major and minor axes of the contact ellipses

The major gear parameters are also the same as those given in Table 1. This example investigates the average ratio a/b of major and minor axes of contact patterns when gear pair with different tooth pressure angles under the ideal assembly condition and axial misalignments without center distance variation.

Case 10. $\Delta\gamma_h = \Delta\gamma_v = 0°$ (ideal assembly condition).

Case 11. $\Delta\gamma_h = -0.05°$, $\Delta\gamma_v = 2.0^{\circ}$.

Table 5 shows the ratio a/b of major and minor axes of the contact ellipses of the spherical gear sets with different tooth pressure angles. It is found that convex pinion meshes with concave gear has a larger ratio of a/b than other mating pairs. Besides, mating gear pairs with axial misalignments result in a smaller ratio of a/b. The gear set with a smaller pressure angle (i.e. 14.5°) results in a larger ratio of a/b than other pressure angle conditions. Moreover, the ratio a/b of assembly case with ideal condition is little larger than the assembly cases with axial misalignments.

6. Conclusions

In this study, the continuous shifting gear cutting is proposed to generate the spherical gears. A continuously positive shifting and then a negative shifting gear cutting can generate the convex spherical gear, and

the reverse order can generate the concave spherical gear. Based on the developed mathematical model of spherical gears, the computer graph of the gear set is plotted, and the TCA is also performed. The instantaneous contact points and kinematic errors of the spherical gear set are calculated. Besides, the contact ellipses and contact patterns of spherical gear sets are also investigated by applying the TCA method, surface separation topology method and the developed computer simulation programs. The simulated results can be concluded by:

1. The meshing of spherical gear set is in point contact, and the contact points of the spherical gear set with axial misalignments and center distance error are located near the center region of tooth surfaces. It means that there is no edge contact for the spherical gear set with axial misalignments. Besides, the locations and sizes of contact patterns of the spherical gear set can be determined. The results are useful to further investigations on the contact characteristic of spherical gear sets.
2. The spherical gear set with a convex tooth mating with a concave tooth has the largest size of contact ellipses, and then the convex tooth mating with spur tooth. A convex tooth mating with a convex tooth has the smallest size of contact ellipses.
3. A spherical gear having a smaller pressure angle (14.5°) results in a larger value of ratio a/b, whereas a larger pressure angle (25.0°) results in a smaller value of ratio a/b. The spherical gear pair with ideal assembly condition has a slightly higher value of ratio a/b than that of the assembly case with axial misalignments.

Acknowledgements

The authors are grateful to the National Science Council of the ROC for the grant. Part of this work was performed under contract No. NSC 94-2212-E-009-028.

References

[1] K. Mitome, T. Okuda, T. Ohmachi, T. Yamazaki, Develop of a new hobbing of spherical gear, Journal of JSME 66 (2000) 1975–1980.
[2] Jon R. Mancuso, Couplings and Joints, second ed., Marcel Dekker, 1999.
[3] S.C. Yang, Mathematical model of a ring-involute-teeth spherical gear with a double degree of freedom, Journal of Advanced Manufacturing Technology 20 (2002) 865–870.
[4] S.C. Yang, C.K. Chen, K.Y. Li, A geometric model of a spherical gear with a double degree of freedom, Journal of Material Processing Technology 123 (2002) 219–224.
[5] Y.C. Tsai, W.K. Jehng, Rapid prototyping and manufacturing technology applied to the forming of spherical gear sets with skew axes, Journal of Materials Processing Technology 95 (1999) 169–179.
[6] C.B. Tsay, Helical gears with involute shaped teeth: geometry, computer simulation, tooth contact analysis, and stress analysis, Journal of Mechanisms, Transmissions, and Automation in Design 110 (1988) 482–491.
[7] C.C. Liu, C.B. Tsay, Contact characteristic of beveloid gears, Mechanism and Machine Theory 37 (2002) 333–350.
[8] Y.C. Tsai, P.C. Chin, Surface geometry of straight and spiral bevel gears, Journal of Mechanism, Transmissions, and Automation in Design 109 (1987) 443–449.
[9] F.L. Litvin, A. Fuentes, K. Hayasaka, Design, manufacture, stress analysis, and experimental tests of low-noise high endurance spiral bevel gears, Mechanism and Machine Theory 41 (2006) 83–118.
[10] F.L. Litvin, Theory of Gearing, NASA Reference Publication 1212, Washington, DC, 1989.
[11] F.L. Litvin, Gear Geometry and Applied Theory, PTR Prentice Hall, Englewood Cliffs, NJ, 1994.
[12] F.L. Litvin, A. Fuentes, Gear Geometry and Applied Theory, second ed., Cambridge University Press, 2004.
[13] W.K. Janninck, Contact surface topology of worm gear teeth, Gear Technology (March/April) (1988) 31–47.